SCEC PROJECT TECHNICAL REPORT 20144: Constraining a long history of paleolake and paleoseismicity at Coachella, CA, using deep borehole samples

Summary

We collected a 33.5-m-deep continuous borehole near the northeastern end of Lake Cahuilla's shoreline at the Coachella structural depression in May 2020 (Fig. 1). The detailed stratigraphic log of the borehole suggests approximately 19 lake highstands (water-lain clay/silt rich units), interrupted by sandy units of the fluvial, deltaic, and recessional bar origin (Fig. 2C–D). Using 13 luminescence and 13 ^{14}C samples from the sandy and clayey units, respectively, we are constraining the lake desiccation and highstand cycle of the ancient Lake Cahuilla (Fig. 2). The corrected luminescence ages show promise and can be used to date lake highstands (shown as L) 6L–12L, 15L, and 17L, with the ages ranging between ~1.4 to 7.6 ka (Fig. 2E). We have improved the accuracy and precision of the single-grain luminescence ages by modelling the environmental dose rate and estimated the water content using different grain sizes across the borehole assuming porosity equates to volumetric water content (Or and Wraith, 2000; Lukas et al., 2012; Nelson and Rittenour, 2015). Several pieces of shells and grass materials were dated for ^{14}C dating at CSUF. However, the ^{14}C dates are either too young (e.g., grasses) or too old (e.g., shells). Our age model for the ancient Lake Cahuilla offers the longest lake history till date, including a wealth of structural information associated with the movement on the southern San Andreas Fault (e.g., Philibosian et al., 2011; Rockwell et al., 2018, 2022).

Preliminary technical science outcomes

- Successful extraction (~86% recovery) of the borehole near the Central trench of the Coachella structural depression, Ave. 44, Indio, CA.
- The borehole represents the longest (past ~8 ka) lake highstand and desiccation chronology of the ancient Lake Cahuilla.
- A total of 19 lake highstands are identified in the borehole stratigraphic log.
- The corrected luminescence ages suggest that the average sedimentation rate is ~2–3 mm/year in the past ~8 ka.

Training, communication, and outreach outcomes

- The project grant supported the salary of one UCLA postdoc.
- Two posters and one oral presentation were made during the SCEC 2020 and 2021 virtual annual meetings.
- A manuscript is in preparation for publication in a peer-reviewed journal.

Project objective and rationale

The project's main objective is to test the hypothesis that the lack of surface rupture since the most recent earthquake (MRE) on the southernmost ~100 km of the San Andreas fault (SSAF) is due to Lake Cahuilla's extended dry period. The average earthquake recurrence interval on this stretch of the SSAF in the previous 1000 years is ~180 years. However, the MRE was recorded around 1726±7 AD, just after the last filling of the ancient Lake Cahuilla in the Salton Trough (Rockwell et al., 2018). Why this stretch of the SSAF remains quiescent for ~300 years is still poorly understood. Some researchers have proposed that lake levels of the ancient Lake Cahuilla modulate the regional stress field (e.g., lake loading and porewater pressure; Luttrell et al., 2007; Brothers et al., 2011) and tie earthquake occurrence to particular lake highstand stages (Rockwell et al., 2018; Rockwell and Klinger, 2019). However, due to limited (~2 ka or younger) lake cycle chronologies as charcoals are sparse and uncertainties in detrital ^{14}C dates (e.g., reservoir effect on

gastropod shells or inheritance of detrital charcoals), the true relationship between loading of the Lake Cahuilla and earthquake cycles has not been adequately evaluated. Besides, solving this connection is critically important to evaluate fault behaviors such as periodicity, segmentation, characteristic versus random rupture behavior (Weldon et al., 2004), and susceptibility to change in transient pore pressure (Luttrell et al., 2007; Brothers et al., 2011). These parameters are, therefore, critical inputs for earthquake hazard-assessment, a key target of SCEC research. They can also significantly improve any future long-term earthquake rupture forecast model's reliability and utility.

Technical report

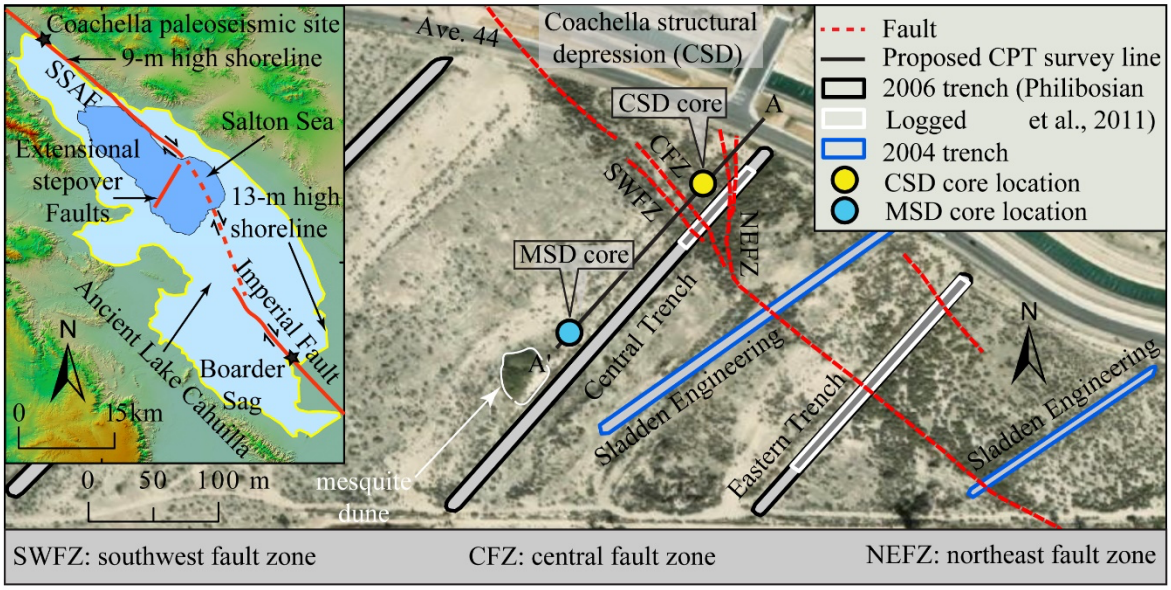

Figure 1. *Map showing the ancient Lake Cahuilla's 13-m shoreline (inset) and location of the CSD borehole, relative to the Central Trench of Philibosian et al. (2009, 2011).*

Our 2020 SCEC research focused on constraining the lake highstand and desiccation cycles of the ancient Lake Cahuilla using a 33.5-m-deep continuous borehole. Since we collected the borehole from the previously studied Coachella structural depression of the Central trench of Philibisian et al. (2011), we named this core CSD (33.728127°N, 116.170041°W; Fig. 1). The CSD borehole is well poised to capture more frequent lake fluctuations near the northeastern edge of Lake Cahuilla shoreline and stratigraphic deformation caused by subsidence on the SSAF. The borehole was extracted using CME-85 continuous core logs and SPT split-spoon sampler (Fig. 2A). Without any plastic liners inserted within the sampler, we could not extract the upper ~6 m of the core (severely disturbed), which was previously logged and dated by Philibisian et al. (2011). To prevent further loss and disturbance to the stratigraphy and limit possible grain mixing, we used 5' x 2.5" transparent plastic liners to recover the rest of the borehole (Fig. 2B). Overall, we recovered about 86% of the borehole.

The individual core segments were immediately warped and capped by double layers of aluminum foils to prevent further sunlight exposure. We opened these core segments at UCLA's Luminescence lab under amber lights. We partially dried the core segments and prepared a stratigraphic log of the borehole under amber light before extracting luminescence samples. We later split the core segments into half and modified the log under bright light aided by their photomosaics (Fig. 2C, D). The stratigraphic log and photomosaics were further complemented by the detailed grain size and shape analysis, which allowed us to confidently

identify the lake highstands (units with relatively high silt and clay and relatively low sand). Grain size and shape analysis was performed at the Quaternary Geology lab of SDSU.

Based on these data, we identified at least 19 possible lake highstands based on distinct clayey/silty horizons, following Philibosian et al. (2011) and Waters (1983; Fig. 2). The clayey/silty (lacustrine) horizons are more compact in the bottom core segments than the top, with clearly visible fine laminations, possibly water-lain. Several small pieces of gastropods and grasses were also found in the lacustrine horizons and collected for ^{14}C dating (Fig. 2E). The lacustrine units are interrupted by thick sandy horizons. Some sandy and silty units that show finning downward and gradual transition to lacustrine units are interpreted as likely deltaic sedimentation resulting from a rising lake level, followed by clay deposition during the full lake (e.g., Rockwell and Klinger, 2019). Additionally, recessional bars are also sandy and usually well sorted. They are likely more prominent in units that show coarsening downward (Fig. 2). We interpret the coarse, in some cases poorly sorted, sandy matrix as likely fluvial in origin. Fluvial processes in terms of sheet wash deposits are presently dominant at the borehole site. They are also reported from other shoreline environments of Lake Cahuilla (Waters, 1983). Aeolian deposits of fine sands are also expected in some units. We are currently improving our stratigraphic interpretation further using grain size, shape, and thin-section analysis.

We sampled selected sandy units by vertically inserting 6" x 1.5" copper tubes inside the liners, which allowed us to exclude any exposed core materials along the edges. We targeted the sandy units primarily because of the suitable grain size (e.g., 185–220 μm) required for single-grain p-IR IRSL dating and the longer sunlight exposure assumed for these grains (Rhodes, 2015). Suitable K-feldspar samples (the ("Super-K" procedure of Rhodes, 2015) were used to determine equivalent doses (D_e). We analyzed approximately 99–127 grains per sample to achieve reasonable certainty and to identify the presence of anomalously young grains. Any anomalously young grains are carefully being treated to estimate the accurate D_e values.

Additional challenges of luminescence dating of borehole samples include asymmetric geologic dose-rates due to non-uniform-grain matrix across distinct stratigraphic units (lacustrine vs. subaerial) and varying water content in the geologic past due to fluctuating potentiometric surface at that location (e.g., Brennan, 2006). For example, we targeted the immediate sandy units bounding the lacustrine units to constrain the start of the lake filling and desiccation (Fig. 2). The rationale behind this approach was to reduce any lag time between lake filling and desiccation imposed by erosion and sedimentation rate. However, the dose-rate contribution of finer grains (e.g., clay, silt, fine sand) is different from the coarser grains (e.g., medium and coarse sand) and also attenuates with distance. We therefore had to correct for the dose-rate variations across stratigraphies using depth-dependent attenuation.

Additionally, water also significantly attenuates the track dose from all but the closest grains (e.g., Brennan, 2006). Since the borehole samples are presently collected from below the groundwater table (i.e., saturated) and are expected to remain saturated in the past, we estimated the volumetric water content from porosity, assuming that all the pore spaces are completely filled with water and water expulsion likely occurred at depth due to sediment overburden (Or and Wraith, 2000; Lukas et al., 2012; Nelson and Rittenour, 2015). Another significant source of uncertainty includes anomalous athermal fading of K-feldspar. All our samples show fading (~2.2–3.1% per decade) at the laboratory timescale (~300 seconds to 7 days). Therefore, we also corrected for the fading. Additional 13 ^{14}C ages were dated but discarded for further analysis since they are either too young (modern) or too old compared to the single-grain luminescence ages in the same stratigraphy (Fig. 2E). Using the published ^{14}C ages (Philibosian et al., 2011; Rockwell et al., 2022), new single-grain p-IR IRSL ages, we reconstructed the long lake chronology of the ancient Lake Cahuilla; dating back to ~8 ka (Fig. 2E). We also estimated the average sedimentation rate between ~2 and

3 mm/year in the past ~8 ka (Fig. 2E). This is similar to what has been reported by other researchers in the study area (Waters, 1983; Philibosian et al., 2011).

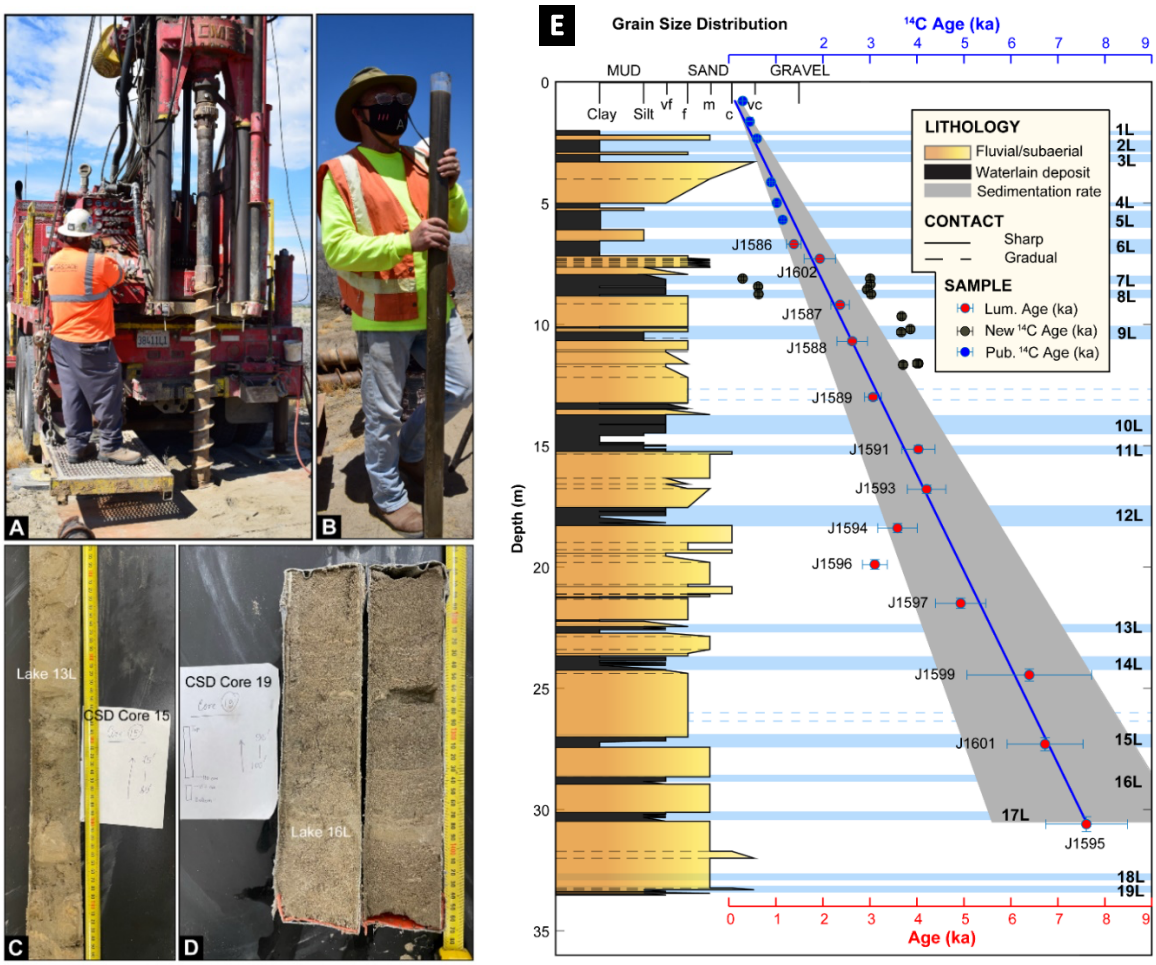

Figure 2. *Field photos showing the drilling of continuous core segments (A) and recovery of the core in plastic liner (B). Photomosaic of core 15 (C) and core 19 (D) highlighting Lake 13 and 16, respectively. (E) New single-grain p-IR IRSL and published (Philibosian et al., 2011; Rockwell et al., 2022) and new ^{14}C ages are plotted with respect to the borehole's depth. Lake Cahuilla's lacustrine units are highlighted in blue bars. The solid blue line with gray shaded area shows the average sedimentation rate ± 1σ (~2–3 mm/year) for the past ~8 ka at the Coachella study site.*

Intellectual merit

The project offers the longest lake filling and desiccation cycles of the ancient Lake Cahuilla in the Salton Trough. These results are crucial to test whether SSAF is susceptible to lake loading and associated porewater pressure or is just a mere coincidence. In addition, the project has intellectual merit to offer long-term sedimentologic context for paleoearthquake and slip rate studies in the Coachella Valley. In combination with geotechnical data (e.g., CPT), borehole data also has the potential to estimate the cumulative vertical displacement at the Coachella site. The new luminescence chronology and analytical

improvements are valuable for providing a means to date deep borehole sediments, especially in contexts where no organic material for ^{14}C exists or are enormously affected by inheritance and ^{14}C reservoir effect.

Broader impacts

This project has provided ample opportunities for research and training at UCLA, SDSU, & CSUF. The project helps develop a series of other projects for the postdoctoral fellow at UCLA. A graduate and two undergraduate students are also being trained under this project. This project is part of a Ph.D. thesis at UCLA and two undergraduate research projects at SDSU and CSUF. Besides, the project contributes directly to address three primary goals of SCEC5: *Science Objectives* of "P5.b.", "P5.c.", and "P5.d."

References

1. Brothers, D., Kilb, D., Luttrell, K., Driscoll, N., Kent, G. 2011. Loading of the Aan Andreas fault by flood-induced rupture of faults beneath the Salton Sea. *Nat. Geosci. 4*, 486–492. https://doi.org/10.1038/ngeo1184.
2. Lukas, S., Preusser, F., Flavio, F.S., Tinner, W. 2012. Testing the potential of luminescence dating of high-alpine lake sediments. Quaternary Geochronology, 8, 23–32. doi:10.1016/j.quageo.2011.11.007
3. Luttrell, K., Sandwell, D., Smith-Konter, B., Bills, B., Bock, Y. 2007. Modulation of the earthquake cycle at the southern San Andreas fault by lake loading. *Journal of Geophysical Research, 112*, 1–15.
4. Nelson, M.S., Rittenour, T.M. 2015. Using grain-size characteristics to model soil water content: Application to dose-rate calculation for luminescence dating. Radiation Measurements, 81, 142–149. http://dx.doi.org/10.1016/j.radmeas.2015.02.016
5. Or, D., Wraith, J.M., 2000. Soil water content and water potential relationships. In: Sumner, M.E. (Ed.), Handbook of Soil Science. CRC Press, London, pp. 53–85.
6. Philibosian, B., Fumal, T.E., Weldon, R.J., Kendrick, K.J., Scharer, K.M., Bemis, S.P., Burgette, R.J., Wisely, B.A. 2009. Photomosaics and logs of trenches on the San Andreas Fault near Coachella, California, in U.S. Geol. Surv. Open-File Report. 2009–1039.
7. Philibosian, B., Fumal, T., Weldon, R. 2011. San Andreas Fault Earthquake Chronology and Lake Cahuilla History at Coachella, California. *Bulletin of the Seismological Society of America*, 101, 13–38. https://doi.org/10.1785/0120100050.
8. Weldon, R. J., Scharer, K. M., Fumal, T. E., Biasi, G. P. 2004. Wrightwood and the earthquake cycle: what a long recurrence record tells us about how faults work, *GSA Today 14, no. 9*, 4–10.
9. Rhodes, E. 2015. Dating sediments using potassium feldspar single-grain IRSL: initial methodological considerations. *Quaternary International 362*, 14–22.
10. Rockwell, T.K., Meltzner, A.J., Haaker, E.C. 2018. Dates of the Two Most Recent Surface Ruptures on the Southernmost San Andreas Fault Recalculated by Precise Dating of Lake Cahuilla Dry Periods. *Bulletin of the Seismological Society of America, 108*, 2634–2649.
11. Rockwell, T.K., Meltzner, A.J., Haaker, E., Madugo, D., White, E. 2019 (in internal review). The Late Holocene History of Lake Cahuilla: Two Thousand Years of Repeated Fillings Within the Salton Trough, Imperial Valley, California. To be submitted to Quaternary Research, December 2019.
12. Waters, M. R. 1983. Late Holocene lacustrine chronology and archaeology of ancient Lake Cahuilla, California. *Quaternary Res. 19*, 373–387, doi: 10.1016/0033-5894(83)90042-X.
13. Brennan, B. J. 2006. 2006. Variation of the alpha dose rate to grains in heterogeneous sediments. *Radiation Measurements, 41*, 1026–1031.

Project	20144							
PI	Seulgi Moon							
date_processed	September 10, 2021							
sample_location	Coachella, CA							
study_site	Coachella paleoseismic site							
fault	San Andreas fault							
latitude	33.73							
longitude	-116.17							
elevation	10 m							
purpose	high-resolution borehole dating							
sample_year	2021							
lab_ID	**sample_name**	**frac_modern**	**frac_err**	**D^{14}C (‰)**	**d^{14}C_err (‰)**	**^{14}C age (yr BP)**	**^{14}C14 age err**	**Material**
250848	CC05.50 Grass .079mgC	0.9731	0.0028	-26.9	2.8	220	25	Grass
250849	CC05.83 Grass .085mgC	0.9339	0.0027	-66.1	2.7	550	25	Grass
250850	CC05.114 Grass .20mgC	0.9328	0.0016	-67.2	1.6	560	15	Grass
250861	CC05.50 FG .20mgC	0.694	0.0013	-306	1.3	2935	15	Fat Gastropod
250862	CC05.74 FG	0.6935	0.0013	-306.5	1.3	2940	20	Fat Gastropod
250863	CC05.95 SG .16mgC	0.6994	0.0015	-300.6	1.5	2870	20	Skinny Gastropod
250864	CC05.114 SG .18mgC	0.6924	0.0014	-307.6	1.4	2955	20	Skinny Gastropod
250865	CC06.53 FG	0.6383	0.0012	-361.7	1.2	3605	20	Fat Gastropod
250866	CC06.106 FG	0.624	0.0012	-376	1.2	3790	20	Fat Gastropod
250867	CC06.118 SG	0.6391	0.0012	-360.9	1.2	3595	20	Skinny Gastropod

250868	CC07.95 FG	0.6107	0.0011	-389.3	1.1	3960	15	Fat Gastropod
250869	CC07.95 SG	0.6128	0.0012	-387.2	1.2	3935	20	Skinny Gastropod
250870	CC07.100 FG .16mgC	0.6362	0.0012	-363.8	1.2	3635	15	Fat Gastropod